# WEDGE PART OF AN ALTAR CROWN SUSPENSION – P-RICH IRON AND HYPOEUTECTOID STEEL – MODERN TIMES – SWITZERLAND

| | |
|---|---|
| **Artefact name** | Wedge part of an altar crown suspension |
| **Authors** | Marianne. Senn (EMPA, Dübendorf, Zurich, Switzerland) & Christian. Degrigny (HE-Arc CR, Neuchâtel, Neuchâtel, Switzerland) |
| **Url** | /artefacts/351/ |

## The object

*Credit HE-Arc CR.*

Fig. 1: P-rich iron wedge part of an altar crown suspension (after Hadzic 2008, 2),

## Description and visual observation

| | |
|---|---|
| **Description of the artefact** | Construction steel used for suspension of an altar crown (Fig. 1). |
| **Type of artefact** | Wedge part of an altar crown suspension in the abbey chapel |
| **Origin** | Abbey of Rheinau, Zürich, Zurich, Switzerland |
| **Recovering date** | 1720 AD |
| **Chronology category** | Modern Times |
| **chronology tpq** | 1720 A.D. |
| **chronology taq** | ---- |
| **Chronology comment** | 1720 AD |
| **Burial conditions / environment** | Indoor atmosphere |


This work is licensed under CC BY-NC-ND 4.0

| | |
|---|---|
| **Artefact location** | Abbey of Rheinau, Zürich, Zurich |
| **Owner** | Canton of Zurich, Zurich |
| **Inv. number** | None |
| **Recorded conservation data** | Not conserved (machine brushed) |

**Complementary information**

Nothing to report.

## Study area(s)

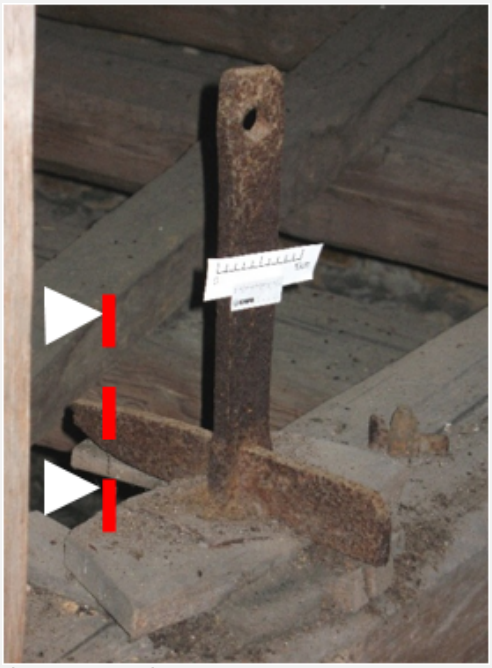

*Credit HE-Arc CR.*

Fig. 2: Location of sampling area,

## Binocular observation and representation of the corrosion structure

Stratigraphic representation: none.

## MiCorr stratigraphy(ies) – Bi

## Sample(s)


This work is licensed under CC BY-NC-ND 4.0

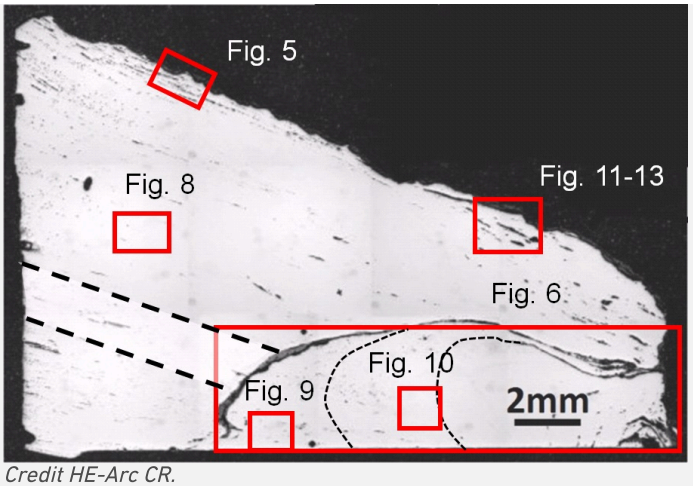

*Credit HE-Arc CR.*

Fig. 3: Micrograph of the cross-section showing the location of Figs. 5 to 13. Steel areas are delimited by black dotted lines,

| | |
|---|---|
| **Description of sample** | This sample is a section from the end of the wedge (Fig. 2). The corrosion crust appears on the top side on Fig. 3. |
| **Alloy** | P-rich iron and hypoeutectoid steel |
| **Technology** | Annealed after (hot) rolling |
| **Lab number of sample** | RHE1-NR |
| **Sample location** | Empa (Marianne Senn) |
| **Responsible institution** | IWT (Naila Hadzic), Wallisellen, Zurich |
| **Date and aim of sampling** | January 2008, material testing and security report |

**Complementary information**

Nothing to report.

## Analyses and results

***Analyses performed:***
Metallography (nital etched and etched with Oberhoffer's reagent), Vickers hardness testing, LA-ICP-MS, SEM/EDS.

## Non invasive analysis

## Metal

The remaining metal (M1) is a P-rich iron (0.3-0.45 mass%) with two zones (M3) consisting of soft, hypoeutectoid steel (C content 0.2 mass%) (Fig. 3 and Table 1). The P-rich iron contains many elongated slag inclusions of various sizes forming parallel rows (Figs. 3 and 5). The number of slag inclusions is higher than in bloomery iron and their distribution is typical for rolled metal. A crack, partially filled by hammer scale and corrosion products, indicates a poor quality welding seam (Fig. 3). Below the inclusions the curve produced by forging is highlighted. In good quality wrought iron slag inclusions are small, uniformly distributed and have identical compositions (Boesenberg 2006, 622). This is not the case in this sample, but can be explained by the rudimentary rolling process of the 18$^{th}$ century. The chemical composition of the slag inclusions shows that iron oxides dominate, beside phosphorus oxide, calcium oxide and silica (Table 2). The composition is typical for slag formed by hearth refining of pig iron (Dillmann and


This work is licensed under CC BY-NC-ND 4.0

L'Héritier 2007). During this process, the pig iron is oxidised. The oxidising elements are Si, P, Mn, V and Cr. The analyzed slag inclusions contain more Fe than most published ones. The high P content is similar to published examples from the 18th century (Dillmann and L'Héritier 2007, 1820). The high calcium oxide content, which is often combined with high silica content, could originate from the addition of both materials while refining the pig iron to better eliminate the P. In one of our measurements, only the silica concentration is high (Table 2). This can be interpreted as resulting from the addition of sand during forging. Etching with Oberhoffer's reagent outlines the thick welding seam (M2, Fig. 6), the rolling direction and the P segregation. Etching with nital mainly shows a ferritic structure (Fig. 7). The grains vary in size (between ASTM grain sizes of 4 to 8) and are recrystallized. The ferrite shows local ghost structures, and includes Neumann bands and some needles (Figs. 8 and 9). These are typical structures of P-rich iron. The ghost structure is formed by a fast recrystallization of P-rich iron after heating above 1000°C. The Neumann bands indicate cold working. The hypoeutectoid steel consists of ferrite with lamellar pearlite (Fig. 10). The average hardness of the metal is HV1 185 (in the Empa test report a mean of HV10 175 was determined). The areas close to the welding seam are harder (ca. HV1 210). The calculated tensile strength based on HV1 175 is about 544N/mm$^2$.

| Elements | Ni/Co | Al | P | Ti | V | Cr | Mn | Co | Ni | Cu | As | Mo | Ag | Sn | Sb | W | C* mass% |
|---|---|---|---|---|---|---|---|---|---|---|---|---|---|---|---|---|---|
| Median mg/kg | 3.1 | < | 3400 | < | 40 | 80 | 20 | 270 | 840 | 340 | 400 | 20 | < | 10 | 10 | < | 0-0.2 |
| Detection limit mg/kg | - | 4 | 65 | 8 | 1 | 10 | 2 | 1 | 3 | 1 | 2 | 3 | 1 | 0.4 | 1 | 3 | - |
| RSD % | 3 | 1 | 16 | - | 168 | 55 | 114 | 6 | 6 | 7 | 19 | 7 | - | 17 | 22 | - | - |

*visually estimated

Table 1: Chemical composition of the P-rich iron. Method of analysis: LA-ICP-MS, Lab Inorganic Chemistry, ETH.

| Structure of inclusion | Env | MgO | $Al_2O_3$ | $SiO_2$ | $P_2O_5$ | $SO_3$ | $K_2O$ | CaO | $TiO_2$ | $V_2O_5$ | $Cr_2O_3$ | MnO | FeO | Total | $SiO_2/Al_2O_3$ |
|---|---|---|---|---|---|---|---|---|---|---|---|---|---|---|---|
| n. d. | steel | 0.8 | 0.7 | 6.1 | 23 | < | < | 9.0 | < | 1.9 | 1.7 | 0.7 | 60 | 105 | 8.3 |
| Glassy matrix | steel | 1.4 | < | 17 | 18 | < | < | < | < | < | < | 0.7 | 66 | 105 | 67 |
| White plates (wustite) | steel | < | < | 1.1 | < | < | < | < | 0.9 | < | < | < | 97 | 101 | 3.4 |
| Droplet (wustite) | steel | < | 1.3 | 0.9 | 1.1 | < | < | 0.6 | < | 2.4 | < | < | 99 | 106 | 0.7 |
| Slag with plates and droplets | steel | 1.0 | 0.6 | 12 | 21 | < | < | 2.7 | < | 0.6 | < | < | 69 | 107 | 20 |
| n. d. | steel | 0.8 | 2.0 | 12 | 29 | 1.0 | 1 | 14 | 0.6 | < | < | 1 | 47 | 109 | 5.7 |
| Wustite in glass | P-rich iron | 0.6 | 0.7 | 6.5 | 17 | 0.8 | < | 4.0 | < | 0.9 | < | 0.9 | 77 | 109 | 9.2 |
| n. d. | P-rich iron | < | 0.8 | 1.3 | 4.6 | < | < | < | 0.6 | 3.0 | 1.5 | < | 94 | 106 | 1.6 |
| n. d. | P-rich iron | 0.8 | 1.1 | 5.4 | 11 | < | < | 3.8 | 0.9 | 3.9 | < | 0.7 | 81 | 108 | 5.1 |
| n. d. | P-rich iron | < | 1 | 1.6 | 3.7 | < | < | 0.8 | 0.8 | 5.3 | 0.7 | < | 84 | 99 | 1.6 |
| n. d. | P-rich iron | 1.2 | < | 8.9 | 13 | < | < | 2.7 | < | 2.3 | 0.7 | 0.9 | 68 | 99 | 18 |
| n. d. | P-rich iron | 0.8 | 1.2 | 8.7 | 23 | < | | 9.8 | < | 0.7 | < | 1.3 | 54 | 99 | 7.6 |

Table 2: Chemical composition of the slag inclusions (mass %). Method of analysis: SEM/EDS, Laboratory of Analytical Chemistry, Empa.


This work is licensed under CC BY-NC-ND 4.0

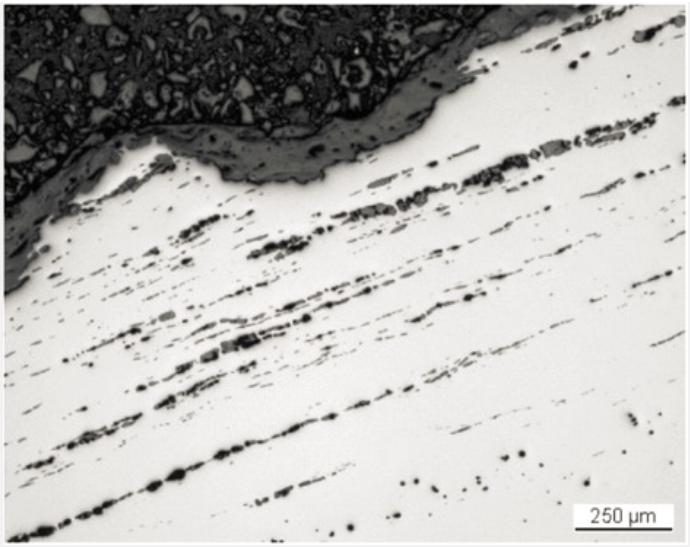


*Credit HE-Arc CR.*

Fig. 5: Micrograph of the metal sample from Fig. 3 (reversed picture, detail), unetched, bright field. In white the metal, in grey the corrosion layer. There are numerous slag inclusions in the metal all orientated to form rows. Some inclusions are empty, probably due to sample preparation,

*Credit HE-Arc CR.*

Fig. 6: Micrograph of the metal sample from Fig. 3 (reversed picture, detail), etched with Oberhoffer's reagent, bright field. The etching shows the P segregation near the welding line and outlines the irregular P distribution in the metal (white P-rich areas, dark P-poor areas),

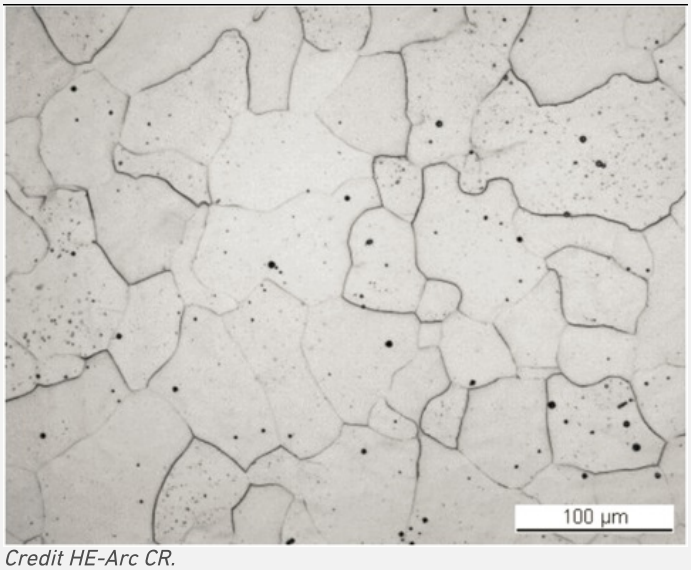


*Credit HE-Arc CR.*

Fig. 7: Micrograph of the metal sample from Fig. 3 (detail), nital etched, bright field. The metal presents a ferritic structure,

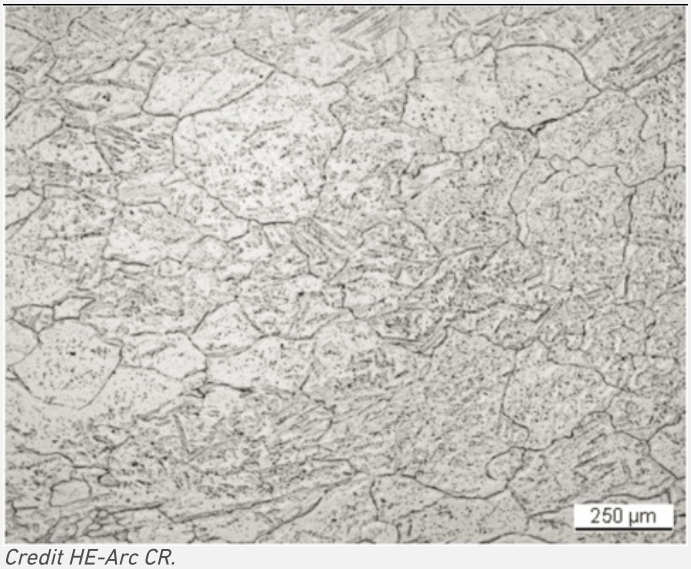


*Credit HE-Arc CR.*

Fig. 8: Micrograph of the metal sample from Fig. 3 (detail), nital etched, bright field. The ferrite shows a ghost structure with needles,


This work is licensed under CC BY-NC-ND 4.0

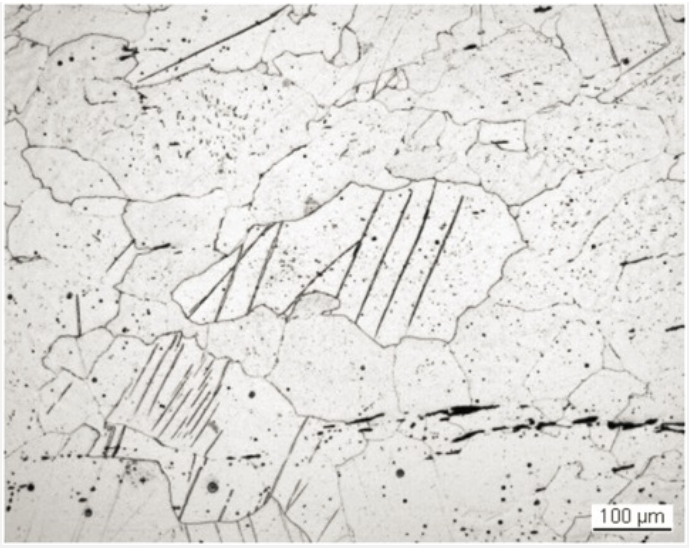


*Credit HE-Arc CR.*

Fig. 9: Micrograph of the metal sample from Fig. 3 (detail), nital etched, bright field. The ferrite grains include Neumann bands,

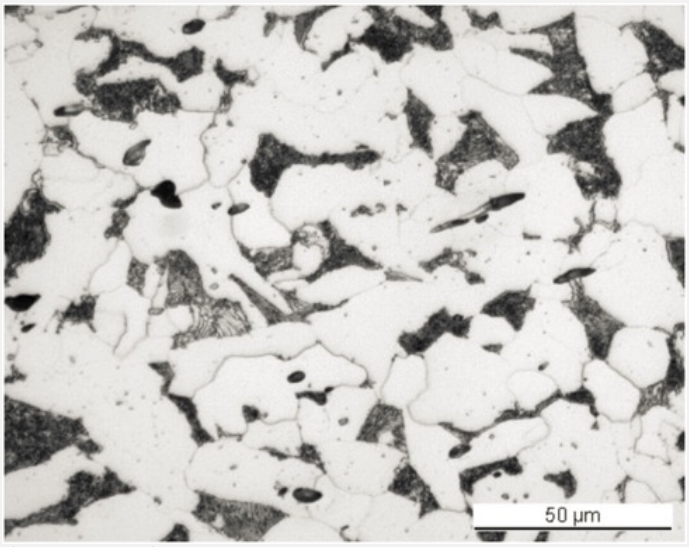


*Credit HE-Arc CR.*

Fig. 10: Micrograph of the metal sample from Fig. 3 (detail), nital etched, bright field. The hypoeutectoid steel is constituted of ferrite in white and lamellar pearlite (in black),

| | |
|---|---|
| **Microstructure** | Recrystallized grains, Newman bands, ghost structure |
| **First metal element** | Fe |
| **Other metal elements** | P |

**Complementary information**

Nothing to report.

## Corrosion layers

The corrosion crust is thin and irregular. It is restricted to one of the three surfaces. In bright field, the corrosion layer seems homogeneous and appears medium-grey with a fissure parallel to the metal surface (Fig. 11). Under polarised light the corrosion products near the metal surface are mostly red-orange (CP3), whereas in the outer layer they appear orange-brown (CP1) (Fig. 12). A dark-brown zone is visible between them (CP2) and contains bright inclusions with a chemical composition similar to wüstite (Table 3). This corresponds to corroded slag inclusions (internal markers). Chemical analysis (Table 3) and elemental mapping (Fig. 13) do not highlight a difference in composition of the corrosion layers, except for the corroded slag inclusions.

| Elements | O | S | Fe | Total |
|---|---|---|---|---|
| Inner part, dark-brown corrosion layer (CP2) | 34 | < | 61 | 96 |


This work is licensed under CC BY-NC-ND 4.0

| | | | | |
|---|---|---|---|---|
| Inner part, orange corrosion products (average of 2 similar analyses) (CP3) | 34 | < | 64 | 99 |
| Bright inclusion | 23 | | 83 | 106 |
| Middle, orange corrosion products | 36 | 0.6 | 64 | 101 |
| Outer orange corrosion layer (average of 3 similar analyses) (CP1) | 34 | 0.7 | 62 | 96 |

Table 3: Chemical composition (mass %) of the corrosion crust (from Fig. 12). Method of analysis: SEM/EDS, Laboratory of Analytical Chemistry, Empa.

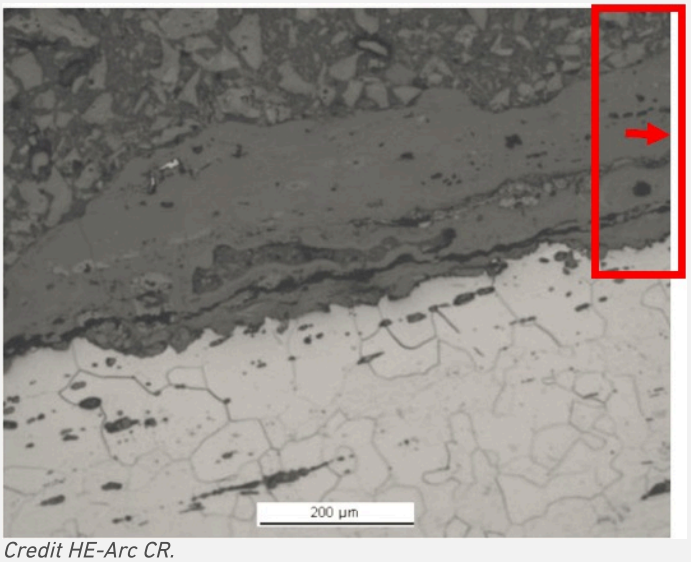


*Credit HE-Arc CR.*

Fig. 11: Micrograph showing the metal - corrosion layer interface from Fig. 3 (reversed picture, detail), unetched, bright field. The grey corrosion layer contains bright inclusion rows. The rectangle marks one part of the mapped area in Fig. 13,

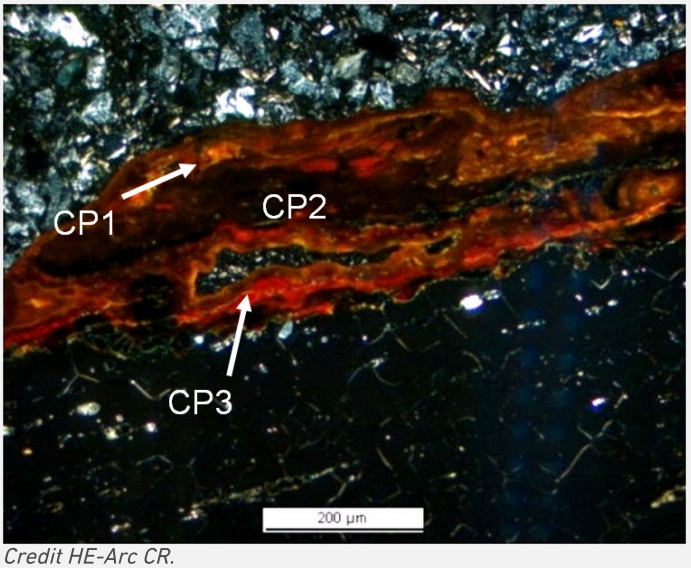


*Credit HE-Arc CR.*

Fig. 12: Micrograph (same as Fig. 11) corresponding to the stratigraphy of Fig. 4, unetched, polarised light. We observe from bottom to top: a red-orange inner corrosion layer (CP3), followed by a dark-brown intermediate layer (CP2) and an orange-brown outer layer (CP1),


This work is licensed under CC BY-NC-ND 4.0

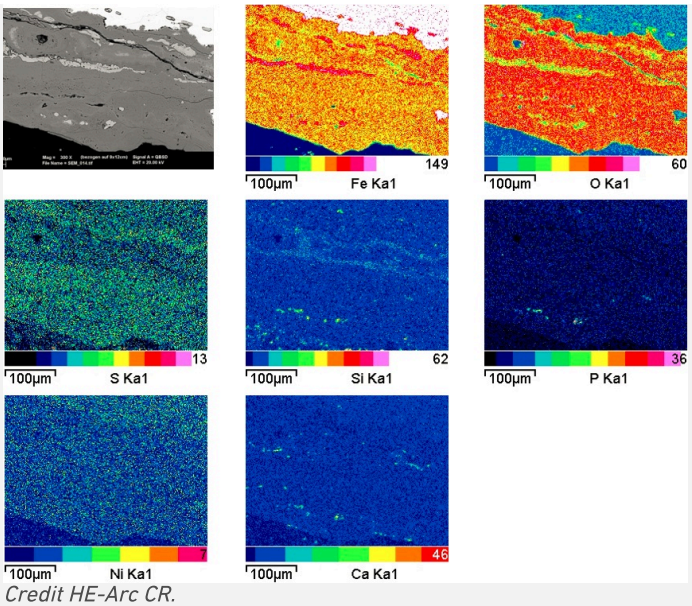


Fig. 13: SEM image, BSE-mode, and elemental chemical distribution of the selected area from Fig. 11 (inversed, detail). Method of examination: SEM/EDS, Laboratory of Analytical Chemistry, Empa,

*Credit HE-Arc CR.*

| | |
|---|---|
| **Corrosion form** | Uniform - pitting |
| **Corrosion type** | ? |

### Complementary information

Nothing to report.

## MiCorr stratigraphy(ies) – CS

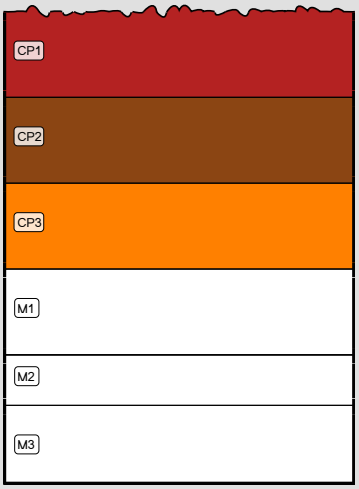


Fig. 4: Stratigraphic representation of the object in cross-section using the MiCorr application. This representation can be compared to Fig. 12.

## Synthesis of the binocular / cross-section examination of the corrosion structure

Corrected stratigraphic representation: none.

## Conclusion


This work is licensed under CC BY-NC-ND 4.0

The wedge was rolled, hammered and annealed from a refined, P-rich wrought iron. It was welded from at least two parts. The C distribution is irregular and shows a zone of soft steel in the middle of the iron. The indoor corrosion seems superficial, but it is possible that the sample surface was cleaned before embedding (Hadzic 2008).

## References


*References on object and sample*

**References sample**

1. Hadzic, N. (2008), Prüfbericht Nr. 448'051, Empa.

*References on analytic methods and interpretation*

2. Boesenberg, J.S. (2006) Wrought iron from the USS Monitor: mineralogy, petrology and metallography. Archaeometry 48-4, 613-631.
3. Dillmann, P., L'Héritier, M. (2007) Slag inclusions analyses for studying ferrous alloys employed in French medieval building: supply o materials and diffusion of smelting process. Journal of Archaeological Science 34, 1810-1823.
4. ASTM E112-13: Standard Test Methods for Determining Average Grain Size.




This work is licensed under CC BY-NC-ND 4.0